Cell and Tissue Research (2021) 383:809–821
https://doi.org/10.1007/s00441-020-03321-7

REGULAR ARTICLE

Sodium alginate/collagen hydrogel loaded with human umbilical cord mesenchymal stem cells promotes wound healing and skin remodeling

Zhenkun Zhang[1] · Zhe Li[1] · Ya Li[1] · Yingying Wang[1] · Minghao Yao[1] · Kun Zhang[1] · Zhenyu Chen[1] · Han Yue[2] · Jijing Shi[3] · Fangxia Guan[1,2] · Shanshan Ma[1]

Received: 23 April 2020 / Accepted: 12 October 2020 / Published online: 7 November 2020
© Springer-Verlag GmbH Germany, part of Springer Nature 2020

Abstract

Stem cell transplantation is a promising therapy for wound healing, but the low retention and survival of transplanted stem cells limit their application. Injectable hydrogels exert beneficial effects in skin tissue engineering. In this study, an injectable hydrogel composed of sodium alginate (SA) and collagen type I (Col) was synthesized as a tissue scaffold to improve the efficacy of stem cells in a full-thickness excision wound model. Our results showed that SA/Col hydrogel was injectable, biodegradable, and exhibited low immunogenicity, which could promote the retention and survival of hUC-MSCs *in vivo*. SA/Col loaded with hUC-MSCs showed reduced wound size ($p < 0.05$). Histological and immunofluorescence results confirmed that SA/Col loaded with hUC-MSCs significantly promoted the formation of granulation, enhanced collagen deposition and angiogenesis, increased VEGF and TGF-β1 expression ($p < 0.05$), and mitigated inflammation evidenced by lower production of TNF-α and IL-1β and higher release of IL-4 and IL-10 ($p < 0.05$). Furthermore, SA/Col loaded with hUC-MSCs significantly lowered the expression of NLRP3 inflammasome-related proteins ($p < 0.05$). Taken together, our results suggest that SA/Col loaded with hUC-MSCs promotes skin wound healing via partly inhibiting NLRP3 pathway, which has potential to the treatment of skin wounds.

Keywords Injectable hydrogel · Mesenchymal stem cells · Wound healing · Tissue remodeling · NLRP3 inflammasome

Introduction

Wound healing plays important roles in protecting against infection and preserving the integrity of skin, and the loss of integrity of skin due to injury or illness may lead to major disability or even death (Rahimi et al. 2020; Singer and Clark 1999). Normal wound healing is a dynamic and interactive process (Zhao et al. 2016). Though most wounds can be self-healed within 1 or 2 weeks, full-thickness wound is an obstacle to tissue repair and regeneration. Over the past years, a number of approaches have been attempted to promote wound healing, such as stem cell transplantation, living skin equivalents into wound tissue, and negative pressure, while optimized therapy needs to be developed (Agabalyan et al. 2019; Chen et al. 2017; Kasuya and Tokura 2014).

Human umbilical cord mesenchymal stem cells (hUC-MSCs) are derived from umbilical cord with low risk of immune rejection, great proliferative capacity, and multilineage differentiation potential (Li et al. 2015; Mushahary et al. 2018). Emerging evidence shows that stem cell transplantation is promising for wound healing, but the low retention and survival of transplanted stem cells limit their application (Huang et al. 2019). One of the major reasons for the low efficiency is the lack of a 3D matrix to support the survival, migration, and development of the transplanted cells (Liang et al. 2013). Therefore, it is important to improve the therapeutic effect of stem cells by optimizing the microenvironment.

✉ Shanshan Ma
mashanshan84@163.com

Fangxia Guan
guanfangxia@126.com

[1] School of Life Sciences, Zhengzhou University, No. 100 Science Avenue, Zhengzhou 450001, Henan, China

[2] Stem Cell Research Center, Henan Provincial People's Hospital, Zhengzhou 450003, Henan, China

[3] Central Lab of the First People's Hospital of Zhengzhou, Zhengzhou 450001, Henan, China

Injectable hydrogels are highly hydrophilic polymers that have been widely applied in various areas of biomedical engineering. Recently, a number of studies have demonstrated that hydrogel-loaded stem cells could facilitate wound healing (Dong et al. 2017; Griffin et al. 2015; Marusina et al. 2020; Xu et al. 2018). Moreover, great efforts have been made to develop in situ injectable hydrogels that can gelate spontaneously and rapidly under physiological conditions and modify the hydrogel niche to meet the needs of different cell cultures and tissue engineering applications.

Sodium alginate (SA), a natural polysaccharide obtained from brown algae, is a traditional material used for injectable hydrogels utilized as wound dressing (Kamoun et al. 2015) and scaffolds (Gao et al. 2019), because of its superior hemostatic capabilities, high hydrophilicity, biodegradability, and excellent biocompatibility. Type I collagen (Col) is the main component of the extracellular matrix that promotes cell proliferation and differentiation (Liu et al. 2018b; Volz et al. 2019). We have previously synthesized SA/Col injectable hydrogel which could prevent the apoptosis of MSCs *in vitro* (Zhou et al. 2019). But whether SA/Col hydrogel could contribute to better microenvironment for hUC-MSCs and improve the therapeutic effect of hUC-MSCs in wound healing still needs to be explored.

Materials and methods

Materials

Mouse fibroblasts cell line L-929 was obtained from the Chinese Academy of Sciences Cell Bank. SA, gluconic acid lactone (GDL), and Col were purchased from Sigma-Aldrich (St Louis, USA). Dulbecco's modified Eagle's medium/Ham's F-12 medium (DMEM/F-12), phosphate-buffered saline (PBS), Dulbecco's modified Eagle's medium (DMEM), fetal bovine serum (FBS), and ELISA kits for IL-1β, IL-4, IL-10, and TNF-α were purchased from Multi Sciences Company (LIANKE, China).

Isolation, culture, and identification of hUC-MSCs

All procedures were conducted in accordance with the ethical standards of the Ethics Committees of the First Affiliated Hospital of Zhengzhou University. The human umbilical cords were obtained from healthy donors following full-term cesarean with prior informed consent. The hUC-MSC derived from Wharton jelly of the human umbilical cord were isolated, cultured, and identified as previously described (Guan et al. 2019). The 3rd–5th passage (P3–P5) cells were cultured and used for experiments.

Fabrication, biocompatibility, and characterization of the SA/Col hydrogel

The SA/Col hydrogel was fabricated by SA, $CaCO_3$, and Col according to previous methods with minor modifications (Zhou et al. 2019). Briefly, SA and Col were respectively dissolved into deionized water (dH_2O) to create 2% SA and 1% Col. Then, the two different solutions in equal volume were mixed. Next, the $CaCO_3$ suspension was put into the SA/Col mix solution, and subsequently into the GDL. Finally, when the ingredients were mixed in an equal volume ratio and reacted for 15 min, the SA/Col hydrogel was successfully obtained in this study.

Toxicity analysis of SA/Col hydrogel

To evaluate the cytotoxicity of SA/Col hydrogel, Cell Counting Kit-8 (CCK-8, US Everbright® Inc., China) was utilized to determine the cell viability (%). The hydrogels were immersed in 24-well plate with DMEM medium and then incubated at 37°C in a moisty atmosphere with 5% CO_2 for 24 h. Then, the sterile extract solution (supernatant of mixed solution collected after incubation of SA/Col hydrogel with DMEM medium for 24 h) was collected. Meanwhile, hUC-MSCs and mouse fibroblasts cell line L-929 were respectively seeded in 96-well plate at 3000 cells in 100 µL corresponding culture medium per well and incubated for 24 h. After incubation, the collected extract solution was diluted by a concentration gradient of 100%, 50%, and 25%. The cell viability of the hUC-MSCs and L-929 were determined by using CCK-8 assay as previously described (Nguyen et al. 2019).

To further investigate the cell viability, the hUC-MSCs loaded in the hydrogels were stained with acridine orange (AO, green) and propidium iodide (PI, red) solution (AO:DMEM/F12:PI = 1:1:50) at 37°C for 15 min and were then observed by fluorescence microscopy (Leica, Germany) (Zhang et al. 2018).

Weight loss of SA/Col hydrogel and biocompatibility *in vivo*

In brief, 100 µL SA/Col hydrogels was lyophilized and immersed in PBS for 1, 3, 5, and 7 days. Then, the hydrogel was taken out and calculated dry weight at different intervals. The weight loss *in vitro* (%) = $(W_0–W_T)/W_0 \times 100\%$, where W_0 denotes initial hydrogel dry weight and W_T denotes the dry weight of the hydrogel at time T after immersion for 1, 3, 5, and 7 days.

To evaluate the loss rate *in vivo*, 100 µL mixed solution was injected subcutaneously in the back of C57/BL6 mice. The remaining hydrogel was separated from the

mice and weighed on 3, 7, 11, and 14 days. The weight loss *in vivo* (%) = $(W_i - W_t)/W_i \times 100\%$, where W_i denotes initial hydrogel wet weight and W_t denotes the wet weight of the hydrogel at time *t* after degradation. The surrounding tissues were separated out on days 3, 7, 11, and 14 and sectioned for hematoxylin and eosin (H&E) staining to assess the biocompatibility of SA/Col hydrogel *in vivo*.

Cell labeling with DiI

To investigate the survival of hUC-MSCs *in vivo*, hUC-MSC were labeled with DiI. Briefly, hUC-MSCs were selected for digestion, and the appropriate cell density was adjusted after resuspension with PBS buffer. The DiI solution was thoroughly mixed, and the cell suspension was incubated in darkness for 20 min before washing off the residual dye. Then, the labeled hUC-MSCs were resuspended with DMEM/F12. Finally, the DiI-labeled hUC-MSCs were transplanted into the lesion, and DiI at day 7 were observed by fluorescence microscopy to evaluate the survival of hUC-MSCs.

Treatment in mice model with full-thickness excision

In order to observe the dynamic of wound closure, male C57/BL6 mice were used to develop full-thickness excision wound models. This study was approved by the Ethics Committees of the Zhengzhou University. The animal procedures were conducted in strict accordance with the National Institutes of Health guidelines for the Care and Use of Laboratory Animals. All manipulations were performed under aseptic condition in this experiment. Briefly, 48 C57/BL6 mice (22-25 g) were intraperitoneally anesthetized with chloral hydrate (10% wt, 100 μL/25 g body weight) and the hair on the mice' back were shaved using an electrical clipper. On the back, 0.8 cm of skin wound in diameter with full-thickness excision was established, and the shaved area was disinfected with 10% Betadine R. Then, all mice were randomly divided into four groups: Control group (DMEM/F-12, 100 μL), SA/Col group (SA/Col hydrogel, 100 μL), hUC-MSCs group (1×10^6 hUC-MSCs, 100 μL), and hUC-MSCs/SA/Col group (SA/Col hydrogel loaded with 1×10^6 hUC-MSCs, 100 μL), and fed in separate cages after injecting subcutaneously around the wound edge, respectively. Digital images were measured on days 0, 7, and 14. The wound area was calculated using ImageJ software. The calculation formula was as follows: (wound area on day 0 − wound area on day "X")/(wound area on day 0) × 100%. The schematic experimental protocol and timeline of experiment were shown in Fig.3a.

Table 1 Related primers' information

Name	Sequence (5′ to 3′)	Length (bp)
Mouse TGF-β1 F	CTCCCGTGGCTTCTAGTGC	133
Mouse TGF-β1 R	GCCTTAGTTTGGACAGGATCTG	
Mouse VEGF F	GCACATAGAGAGAATGAG CTTCC	105
Mouse VEGF R	CTCCGCTCTGAACAAGGCT	
Mouse β-actin F	TTGCTGACAGGATGCAGAAG	147
Mouse β-actin R	TGATCCACATCTGCTGGAAG	

Histological examination

On day 9 and day 14 after injury, specimens were taken from mice of each group. These tissue samples were fixed in 4% paraformaldehyde (PFA), embedded in paraffin, and then cut into 3-μm-thick sections by pathological microtome (Leica, Germany). The sections were then stained with H&E and Masson's trichrome before examined under microscope (Leica, Germany). And, the quantitative result of Masson trichromatic staining was quantified with ImageJ software (NIH, USA).

Immunohistochemical and immunofluorescent staining

For immunohistochemical staining, 3-μm-thick skin sections were deparaffinized and washed three times by deionized water for 5 min. Then, the microwave oven was used for antigen retrieval before being blocked with 3% serum for 30 min at room temperature. Next, the slides were incubated with primary CD31 antibody (Abcam, USA, 1:2000). Subsequently, they were incubated with HRP-labeled secondary antibody (Servicebio, China, 1:200). All staining were imaged, and five different microscopic fields for each sample were examined by two blinded observers.

Immunofluorescence was also performed after the fixation of sections in 4% PFA at − 20°C. These slides were taken from each group on day 7 and day 9 after injury. 5-ethynyl-2′-deoxyuridine (EdU), keratin 6 (K6) (Proteintech, China, 1:200), α-SMA (Wanleibio, China, 1:200), and iNOS (Proteintech, China, 1:200) antibodies were used for immunofluorescent staining. Nuclei were stained with DAPI (Solarbio, China). Immunofluorescence images were captured under fluorescence microscopy (Leica, Germany).

Quantitative real-time PCR analysis

Total RNA was isolated by TRIzol reagent on day 9 after injury. Subsequently, qRT-PCR was performed by a quantitative real-time PCR detection system (LightCycler® 480II, Roche, Switzerland) to analyze the gene expression of the

vascular endothelial growth factor (VEGF) and transforming growth factor-β1 (TGF-β1). Moreover, the primers are listed in Table 1.

Detection of inflammatory factors by ELISA

The levels of inflammatory cytokines were detected by enzyme-linked immunosorbent assay (ELISA). The peripheral blood of anesthetized mice were taken from each group of mice and placed for 6 h at room temperature to obtain a supernatant on 7 days after the operation. The serums were acquired after centrifuging the supernatant at 3000 rpm for 20 min. The release of TNF-α, IL-1β, IL-4, and IL-10 was measured by ELISA according to the manufacturer's instructions (MULTI SCIENCES, China).

Western blot

Total proteins from the wound tissues were extracted and separated in SDS-PAGE. Western blot was used to detect the related proteins expression of NLRP3 signaling. The membranes were incubated with the primary antibodies rabbit polyclonal anti-caspase-1 (Wanleibio, China, 1:1000), NLRP3 (Wanleibio, China, 1:1000), IL-1β (Wanleibio, China, 1:1000), and β-actin (Proteintech, China, 1:1000). After being kept overnight at 4°C, the membranes were further marked with the HRP-conjugated goat anti-rabbit secondary antibody (Proteintech, China, 1:2000), and the protein expression was examined by a molecular imaging luminescence system (Azure Biosystems, USA). The quantitative analysis of protein bands was quantified with ImageJ software (NIH, USA).

Statistical analysis

All values are presented as mean ± standard deviation (SD), and the statistical differences between two groups were determined using the Student's unpaired *t* test. Differences among the groups were assessed using one-way ANOVA. *p* Value less than 0.05 was regarded to be significant (significance levels: $*p < 0.05$, $**p < 0.01$, and $***p < 0.001$).

Results

Synthesis and characterization of the SA/Col hydrogel

In the present study, the survival rates of hUC-MSCs and L929 were maintained above 90% (Fig. 1 a and b) when they were cultivated with different extracts of SA/Col hydrogels (100%, 50%, and 25%) for 24 and 48 h, which suggested that SA/Col hydrogels exhibited favorable cytocompatibilty on the growth of hUC-MSCs and L929.

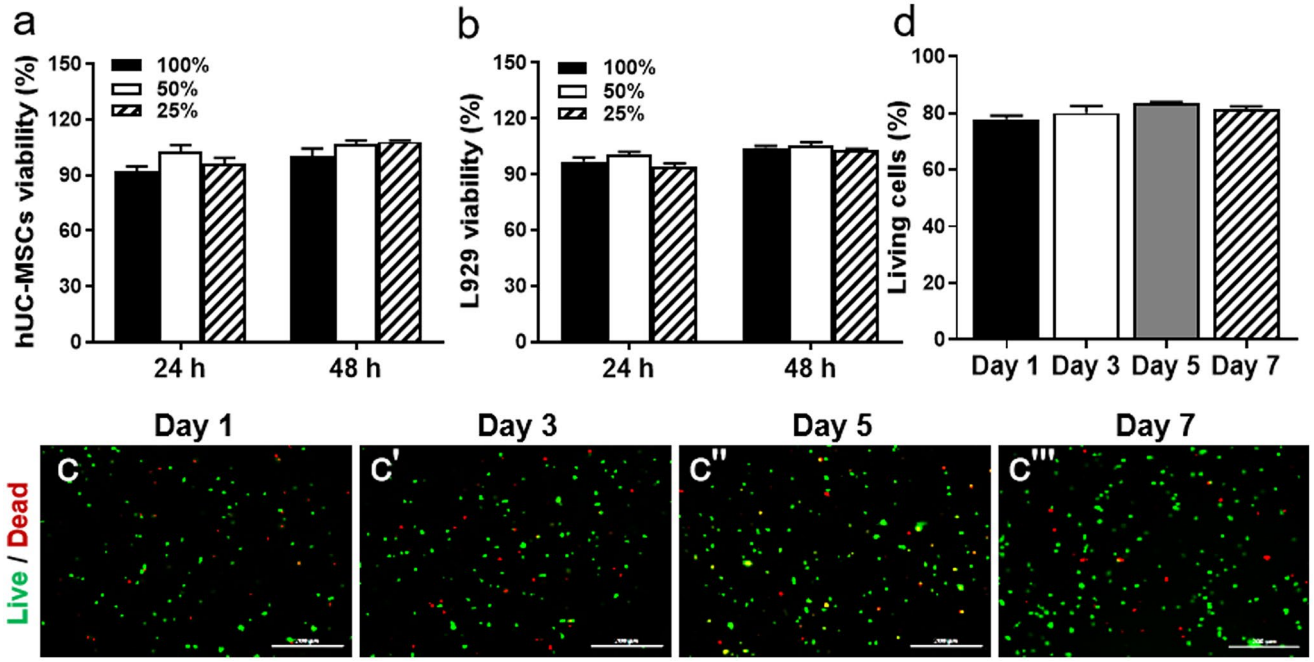

Fig. 1 Biocompatibility of SA/Col hydrogel. The toxicity of hydrogel extract on hUC-MSCs and L929 cells was determined by CCK-8 assay at 24 and 48 h; 100%, 50%, and 25% represented the concentration of the hydrogel extract respectively (a, b). AO (green, live cells) and PI (red, dead cells) staining for hUC-MSCs (c-c'''), scale bar = 200 μm. Cell viability analysis of encapsulated hUC-MSCs in the hydrogels was performed by live/dead assay (d)

To further evaluate the cytocompatibility of SA/Col hydrogel, SA/Col hydrogels loaded with hUC-MSCs were stained by AO and PI at 1, 3, 5, and 7 days. Obviously, SA/Col hydrogel presented a good cytocompatibility to hUC-MSCs, with living cell rate about 80% in all 7 days (Fig. 1 c-c''' and d). The results showed that SA/Col hydrogel had no cytotoxicity to the growth of hUC-MSCs and L929, which provided a comfortable living environment for cells.

Then, the weight loss of SA/Col hydrogel *in vitro* and *in vivo* was further measured. As shown in Fig. 2a, SA/Col hydrogel displayed a relatively slow degradation rate within 7 days *in vitro*. *In vivo*, SA/Col solution rapidly formed in situ hydrogel under the skin with almost no inflammatory cells in the tissues around hydrogels examined by H&E staining, and then gradually degraded within 14 days (Fig. 2 b-b''', c-c''' and d). The degradation trends of hydrogels were roughly similar to that *in vitro*. These results proved that the SA/Col hydrogel was injectable, biodegradable, and low immunogenicity *in vivo*.

SA/Col hydrogel promotes the growth of hUC-MSCs *in vivo*

The growth of hUC-MSCs *in vivo* was detected by DiI fluorescence staining. Different numbers of DiI stained hUC-MSCs were observed in hUC-MSCs group and SA/Col/hUC-MSCs group at the site of injury (Fig. 3), while the SA/Col/hUC-MSCs group exhibited more positive cells than hUC-MSCs group. This was consistent with our results *in vitro* and these findings proved that SA/Col hydrogel greatly increased the retention and survival of hUC-MSCs *in vivo*.

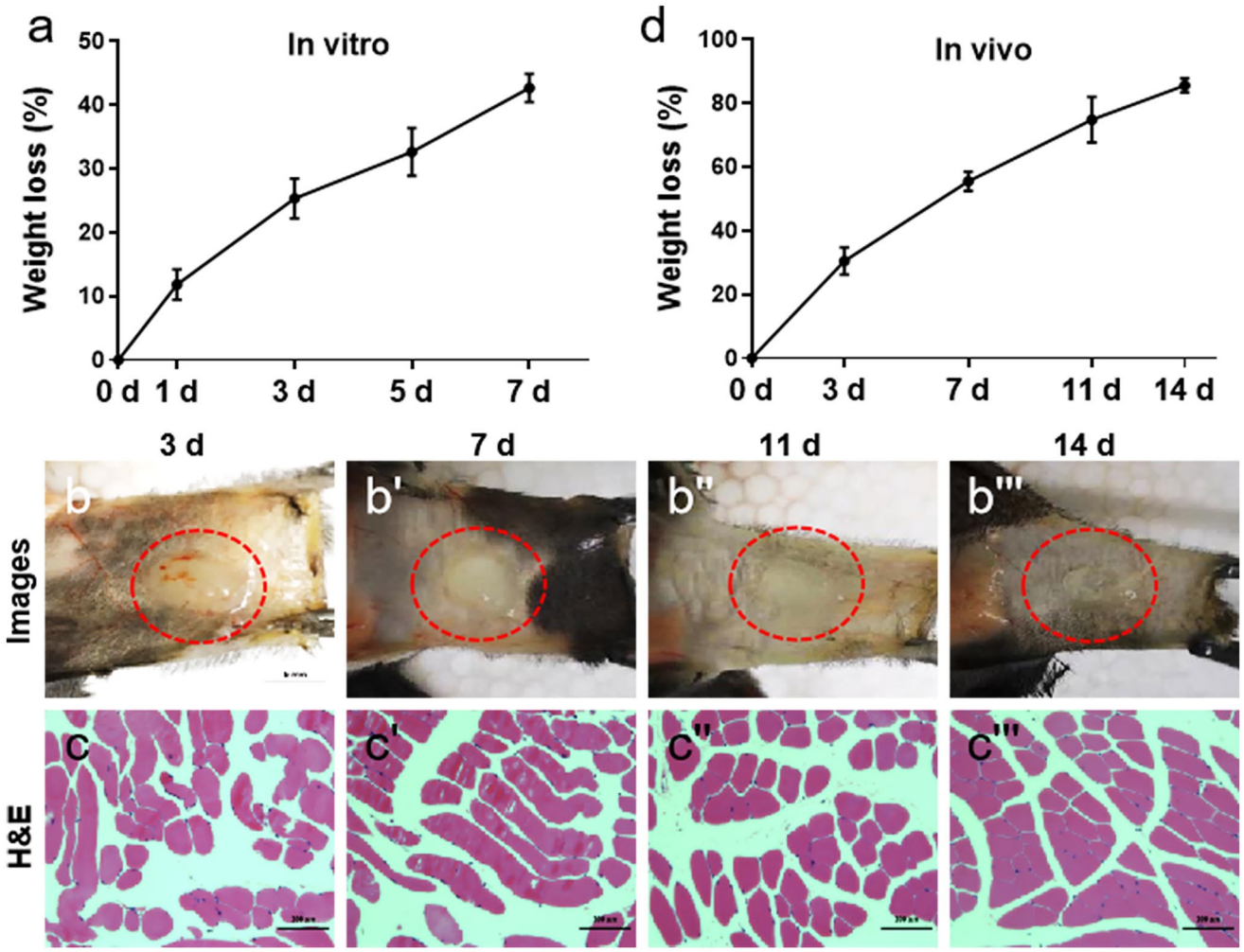

Fig. 2 The weight loss of SA/Col hydrogel both *in vitro* and *in vivo*. Weight loss of hydrogel at different time points *in vitro* (a). Images of SA/Col hydrogels on 3, 7, 11, and 14 days after subcutaneous injection (b-b''', scale bar = 5 mm) and H&E staining of the muscular tissue around the hydrogels at different time points *in vivo* (c-c''', scale bar = 100 μm). Statistical analysis of the degradation of hydrogel on 3, 7, 11, and 14 days *in vivo* (d)

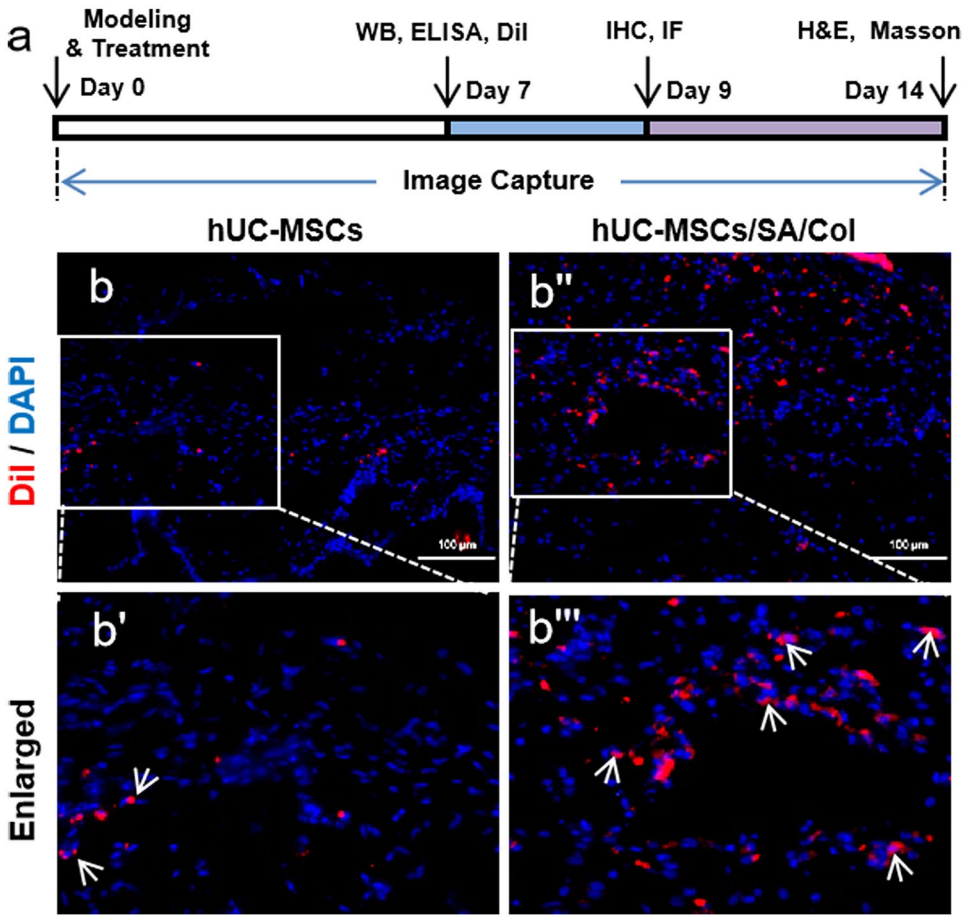

Fig. 3 The growth of hUC-MSCs *in vivo*. Schematic experimental protocol and timeline for experiment (a). DiI staining (red) of the skin wound tissue for hUC-MSCs located at the wound after injecting SA/Col/hUC-MSCs and hUC-MSCs for 7 days (b-b'''). The white arrows indicated DiI-labeled hUC-MSCs at 7 days of treatment. Cell nuclear (blue) was labeled by DAPI. Scale bar = 100 μm

SA/Col hydrogel loaded with hUC-MSCs accelerates wound closure

As shown in Fig. 4a-l, hUC-MSCs/SA/Col group exhibited substantial reduction of wound area compared with other 3 groups on day 14 after treatment ($p < 0.001$), which was confirmed by the quantitative wound area at day 14 in the hUC-MSCs/SA/Col group (1.62 ± 0.43%), hUC-MSCs group (20.52 ± 1.57%), SA/Col group (30.85 ± 1.62%), and Control group (43.93 ± 2.04%) in Fig. 4m. Our results showed that SA/Col hydrogel loaded with hUC-MSCs accelerated wound closure.

SA/Col hydrogel loaded with hUC-MSCs promotes tissue remodeling

H&E was performed to assess the repair of wound at 14 days after treatment. As shown in Fig. 5a-a''', hUC-MSCs/SA/Col group exhibited more granulation and denser structure at the wound site. Collagen deposition is an indicator which reflects the wound repair. So, Masson's trichrome staining was used to determine the formation of collagen, which was dyed blue. In addition, there was significant loss of collagen in Control group, while the collagen deposition in hUC-MSCs/SA/Col group was significantly higher compared to other three groups (Fig. 5 b-b''' and c, $p < 0.01$). And, the collagen fibers in hUC-MSCs/SA/Col group exhibited more orderly arrangement than other groups. These results indicated that SA/Col hydrogel loaded with hUC-MSCs could accelerate wound closure and tissue remodeling by increasing collagen deposition.

hUC-MSCs/SA/Col promotes the proliferation of fibroblast and keratinocyte cells

To further investigate the proliferation of fibroblast and keratinocyte, EdU staining and K6 immunofluorescence were examined, respectively. As shown in Fig. 6 a-a''' and c, hUC-MSCs/SA/Col group displayed more EdU-positive cells than those in other groups ($p < 0.01$). K6 is an indicator of keratinocyte proliferation, the expression of K6 in the hUC-MSCs/SA/Col group was evidently higher than the other three groups ($p < 0.001$, Fig. 6 b-b''' and d). In addition, TGF-β1 can promote fibroblasts to transform into myofibroblasts, and regulate the re-epithelialization process by enhancing keratinocyte migration (Martin 1997; Reynolds et al. 2005). Therefore, qRT-PCR was used to detect the mRNA expression level of TGF-β1. As shown in Fig. 6e, the mRNA expression

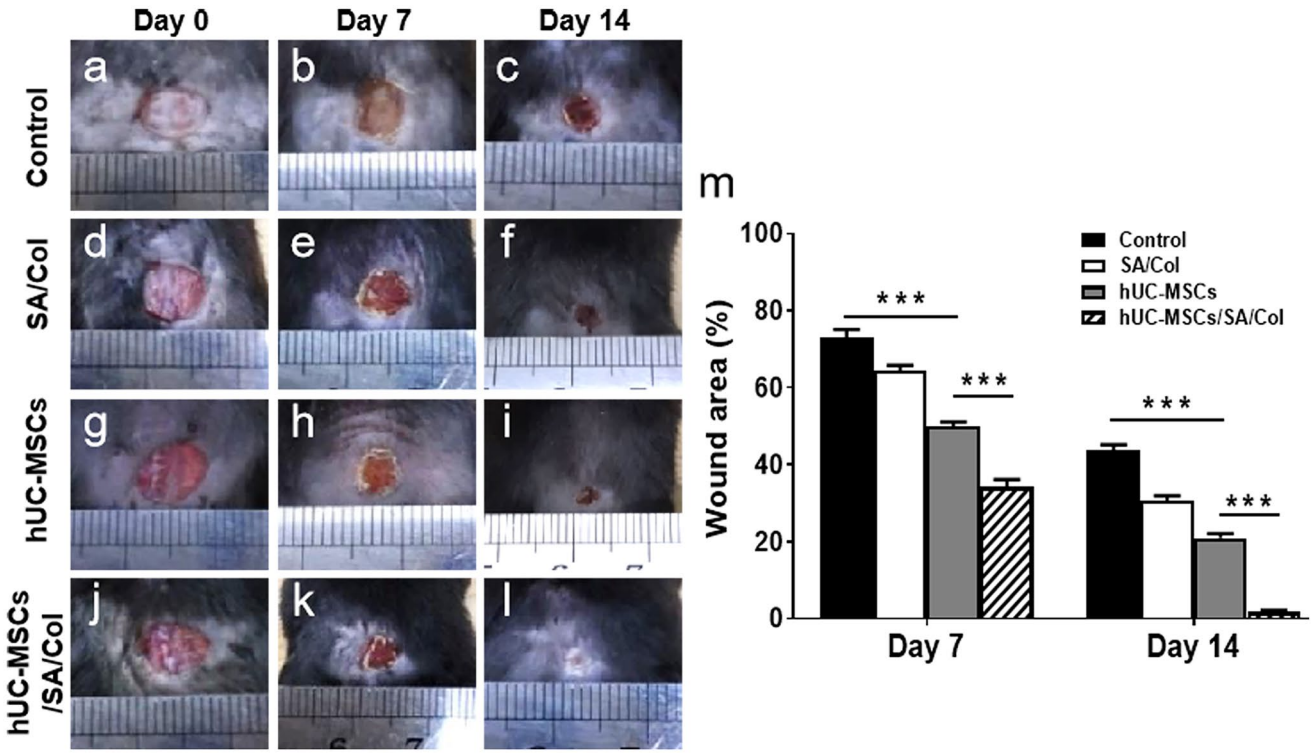

Fig. 4 SA/Col hydrogel loaded with hUC-MSCs accelerated wound healing. General observations at different time point after treatment (**a-l**) and wound area restriction at day 7 and day 14 in different groups (**m**). Data were presented as mean ± SD. ***$p < 0.001$

of TGF-β1 was significantly up-regulated in the hUC-MSCs/SA/Col group ($p < 0.05$). These results revealed that SA/Col hydrogel loaded with hUC-MSCs could promote epidermis and dermis remodeling after wound healing and accelerate the maturation of keratinocytes.

hUC-MSCs/SA/Col hydrogel enhances angiogenesis

Angiogenesis is also a crucial factor in the healing stage of the wound. To assess the angiogenesis during the healing, CD31 immunohistochemistry, α-SMA immunofluorescence staining, and mRNA expression of VEGF were detected respectively in each group. hUC-MSCs/SA/Col group displayed more CD31-positive stained vessels and increased fluorescence intensity of α-SMA at day 9 compared to those in other three groups, respectively ($p < 0.05$, Fig. 7a-a''', b-b''', c, and d), which was accompanied by higher VEGF expression in hUC-MSCs/SA/Col group ($p < 0.01$, Fig. 7e). So, our findings indicated that hUC-MSCs/SA/Col hydrogel could enhance angiogenesis in wound healing.

SA/Col hydrogel loaded with hUC-MSCs inhibits inflammatory response

Inflammation plays vital roles in tissue regeneration (Goren et al. 2018). iNOS, a marker of inflammation, was investigated to detect the inflammation in the wound at day 7 after treatment. As shown in Fig. 8 a-a''' and b, hUC-MSCs/SA/Col significantly decreased the fluorescence intensity of iNOS compared with other 3 groups ($p < 0.01$). In addition, SA/Col/hUC-MSCs greatly mitigated inflammation evidenced by lower production of TNF-α and IL-1β, while higher release of IL-4 and IL-10 ($p < 0.05$, Fig. 8 c and d).

To further explore the mechanism of SA/Col/hUC-MSCs in wound healing, western blot was preformed to evaluate the expression of inflammasome components in the injured skin tissue, including NLRP3, caspase-1, as well as the downstream inflammatory factor IL-1β. As shown in Fig. 8 e and f, the expressions of NLRP3, caspase-1 and IL-1β were significantly decreased in hUC-MSCs/SA/Col group compared with other three groups ($p < 0.05$). To conclude, hUC-MSCs/SA/Col could inhibit inflammation to promote wound healing by suppressing NLRP3 signaling pathway.

Discussion

Aberrant wound healing is an urgent medical problem, which has made substantial burden on patients, families, and the whole society (Hersant et al. 2019). In this study, we fabricated an in situ injectable hydrogel by crosslinking

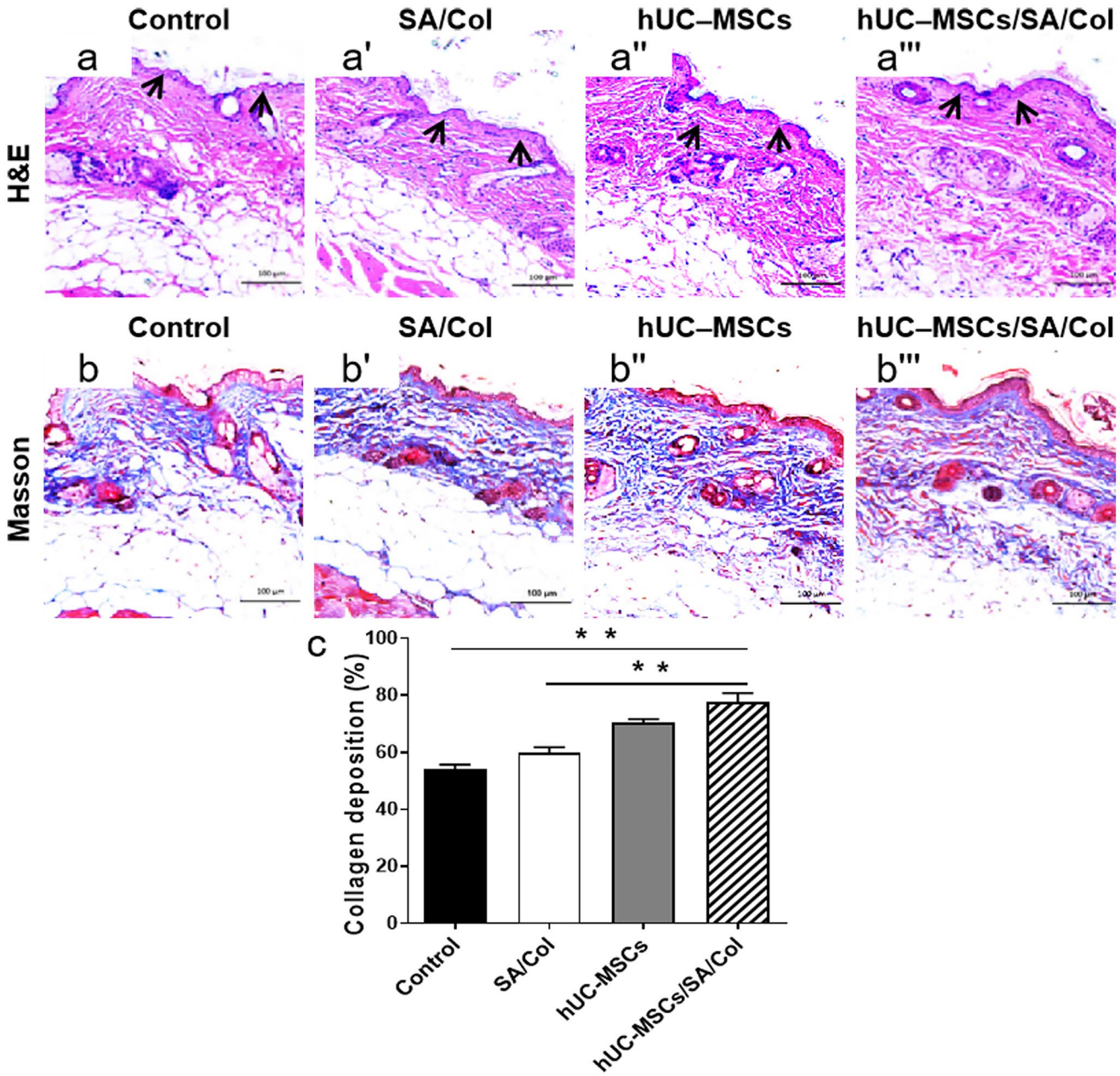

Fig. 5 SA/Col hydrogel loaded with hUC-MSCs promoted tissue remodeling. H&E staining of full-thickness wounds. Black arrows: epidermal layer (a-a'''). The synthesis and deposition of collagen in the wounds of different groups at 14 days after the operation were examined by using Masson's trichrome staining (b-b'''). The collagen fibers were dyed blue and the muscle fibers were dyed red. Collagen deposition in each group (c). Scale bar = 100 μm. $^{**}p < 0.01$

SA and Col with GDL, which is biodegradable and can promote the proliferation and angiogenesis in regenerated tissue when loaded with hUC-MSCs and further accelerate wound healing. In addition, our findings also showed that SA/Col/hUC-MSCs greatly mitigated inflammation partly via the inhibition of NLRP3 signaling pathway.

Stem cell has emerged as a promising therapy for wound healing, with the potential to restore tissue to its pre-injured state. Several mechanisms have been proposed to address the therapeutic function of MSCs, such as direct differentiating into vascular endothelial cells to substitute the injured cells, promoting angiogenesis, modulating the immune response, and secreting paracrine cytokines (Liu et al. 2018a; Spees et al. 2016). While, one of the key factors that determines the stem cell therapeutic effects is its survival in the niche. Injectable hydrogels seem to be a good choice because their extracellular matrix like structure improves cell adhesion and proliferation, and

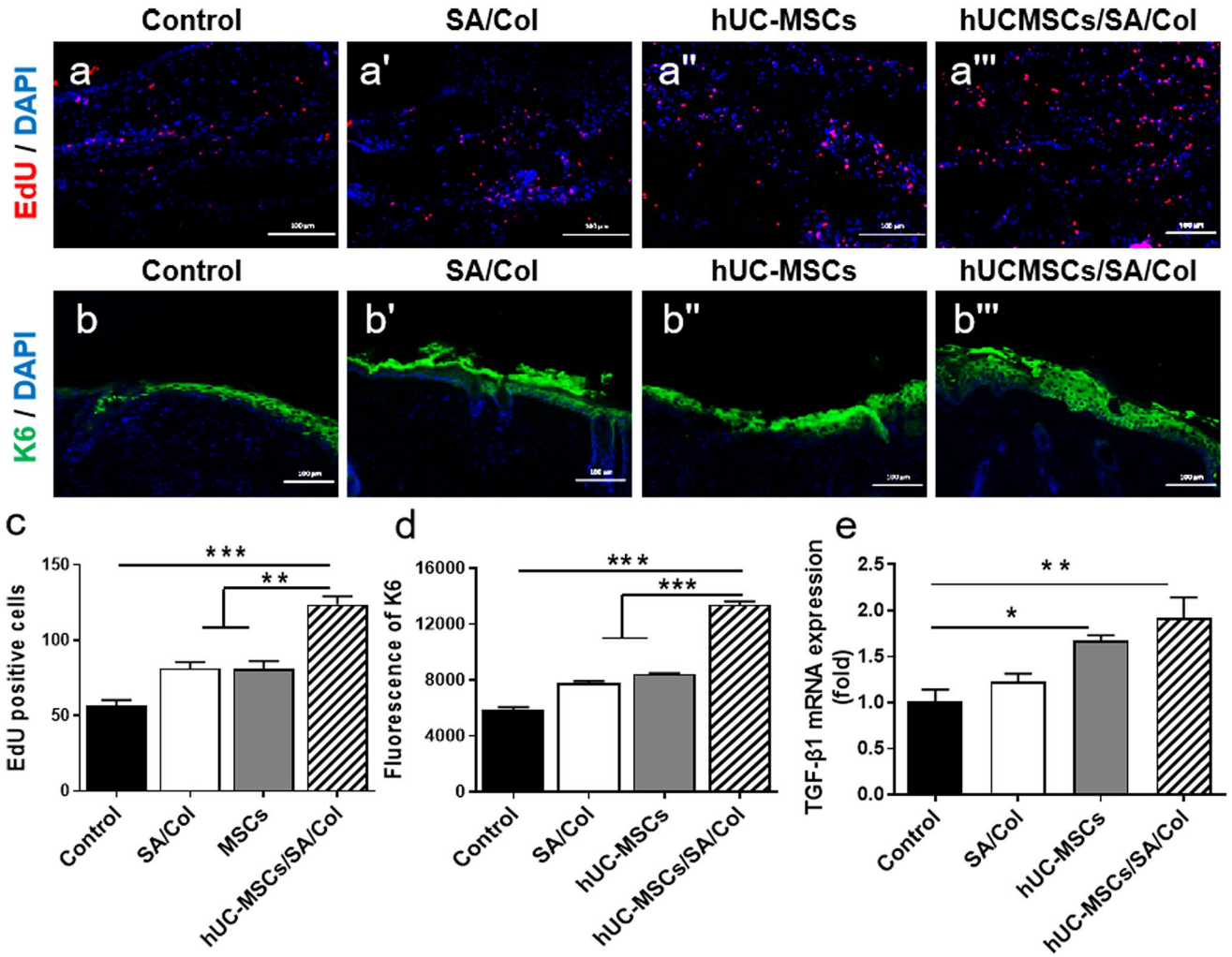

Fig. 6 SA/Col hydrogel loaded with hUC-MSCs promoted skin cell proliferation. Representative images of EdU (a-a''') and K6 (b-b''') immunofluorescence staining. Quantification analysis of EdU-positive cells and K6 expression (c, d). Quantitative analysis the mRNA expression level of TGF-β1 (e). Scale bar = 100 μm. Data were presented as mean ± SD. *$p < 0.05$; **$p < 0.01$; ***$p < 0.001$

maximizes cell viability (Gilarska et al. 2019). Our present study showed that SA/Col hydrogel had no cytotoxicity to the growth of hUC-MSCs *in vitro* and provided a comfortable microenvironment for the survival of implanted hUC-MSCs in the wound site.

Wound healing is an intricate process comprised of different stages, including inflammation, cell proliferation, and matrix remodeling. Aberrations in any of the stage may lead to delayed wound closure. Re-epithelialization and angiogenesis are critical factors in wound recovery. Our previous studies showed that BMSC-laden gelatin hydrogel could accelerate dermal wound healing (Yao et al. 2019). The proliferation and differentiation of keratinocytes are also key steps of epithelialization. K6, an indicator of keratinocyte proliferation, determines the quality of the re-epithelialization level of the wound. In this study, we found that SA/Col hydrogel loaded with hUC-MSCs could promote wound closure by improving cell proliferation, re-epithelialization capability, collagen deposition, and tissue remodeling.

Angiogenesis, the formation of new blood vessels via sprouting, is a complex process of endothelial cells migrating from the original blood vessels, forming new connections to increase the vascular network (Chappell et al. 2012). Interestingly, adult vascular endothelial cells are essentially stationary; however, during physiological processes such as wound healing, they are activated to restart angiogenesis (Dvorak 2015). Our findings showed that SA/Col hydrogel loaded with hUC-MSCs significantly promoted angiogenesis and maturation by increasing CD31 and α-SMA expression respectively in proliferative period. VEGF is an effective proangiogenic growth factor which can promote the formation of microvascular and accelerate neovascularization in the proliferation stage (Wang et al. 2019). While in the remodeling stage, TGF-β1 is the strongest known

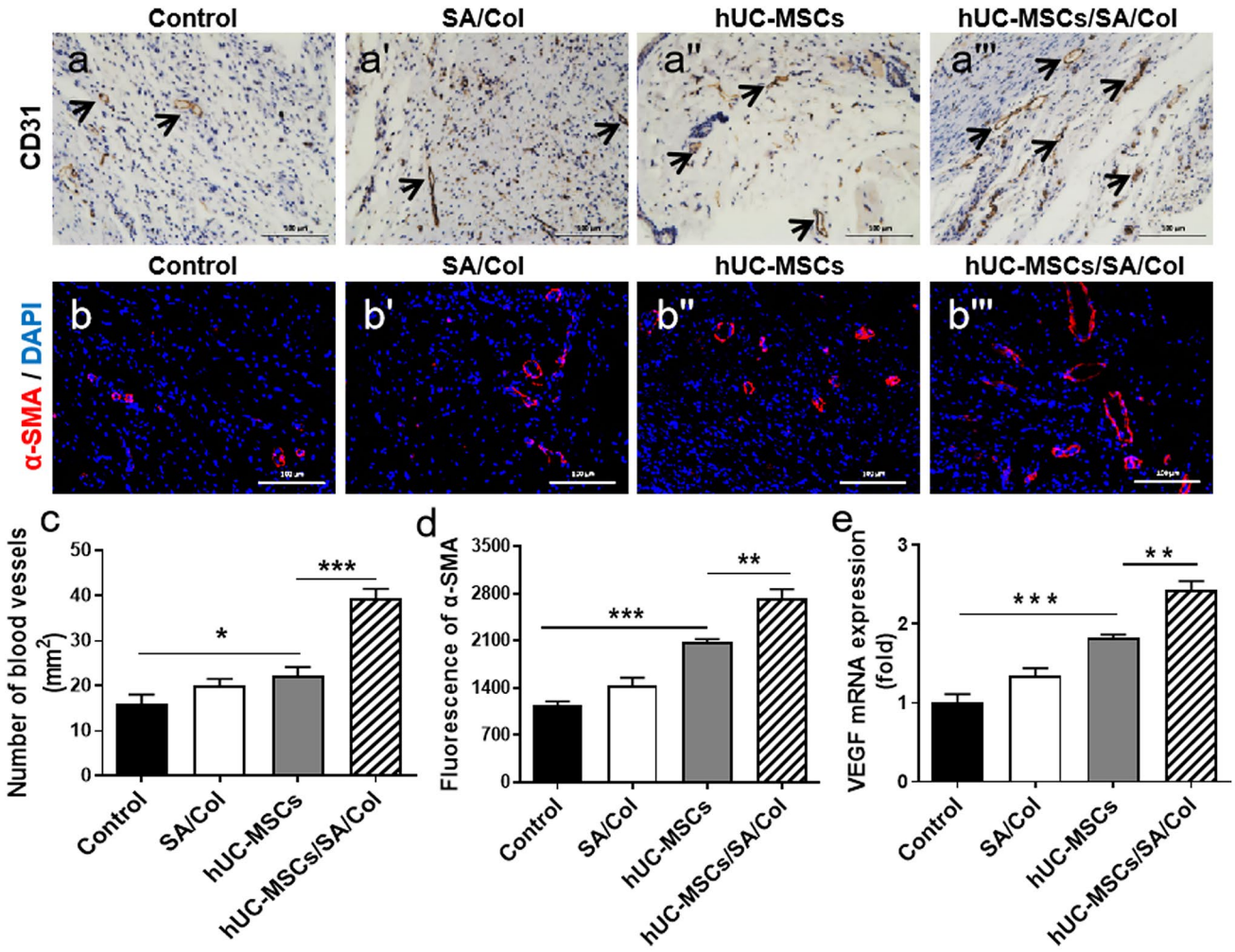

Fig. 7 hUC-MSCs/SA/Col hydrogel facilitated angiogenesis. Representative images of CD31 (a-a''') and α-SMA immunofluorescence staining (b-b'''). Quantification analysis of vessels (c). Quantification analysis of fluorescence intensity of α-SMA (d). Quantitative analysis the mRNA expression level of VEGF (e). Scale bar = 100 μm. Data were presented as mean ± SD. *$p < 0.05$; **$p < 0.01$; ***$p < 0.001$

fibrosis-promoting factor to affect granulation tissue formation, myofibroblast transformation and re-epithelialization (Chen et al. 2015). Alexandre et al. found that TGF-β could increase MSC differentiation and fibroblast differentiation into myofibroblasts (Vallee and Lecarpentier 2019). In this study, we found that SA/Col hydrogel promoted hUC-MSCs to secrete VEGF and TGF-β1, resulting in a significant difference in α-SMA expression, re-epitheliazation, and angiogenesis in the hUC-MSCs/SA/Col group.

Previous study has reported that inflammation is an important process for tissue regeneration, such as neural repair, skin regeneration, and angiogenesis (Rathinam and Chan 2018; Sakai and Shichita 2019). Many bioactive materials (such as SA, Col, bioglass, etc.) have been demonstrated to be able to regulate inflammation response in wound healing (Chin, et al., 2019). Ma et al. found that SA hydrogel had suppression effects on the pro-inflammatory environment in a diabetic mouse skin damage model by stimulating macrophages to polarize into M2 and promoting wound healing (Ma et al. 2020). Wang found that drug-loaded SA hydrogel exhibited better anti-inflammation ability by inhibiting the aggregation of macrophages (Wang et al. 2020). In addition, MSCs loaded with gelatin microcryogels could attenuate renal fibrosis by reducing the mRNA levels of TNF-α and IL-6 (Geng et al. 2019). In our study, iNOS, which is mainly expressed in vascular smooth muscle cells (VSMCs) and significantly induced by inflammation, was used to analyze the activation of inflammation. Our results showed that hUC-MSCs/SA/Col significantly inhibited the expression of iNOS and reduced inflammatory processes by decreasing the release of TNF-α and activating IL-4 and IL-10 secretion in the wound.

NLRP3 inflammasome mediated signaling pathway plays critical roles in inflammatory process. NLRP3

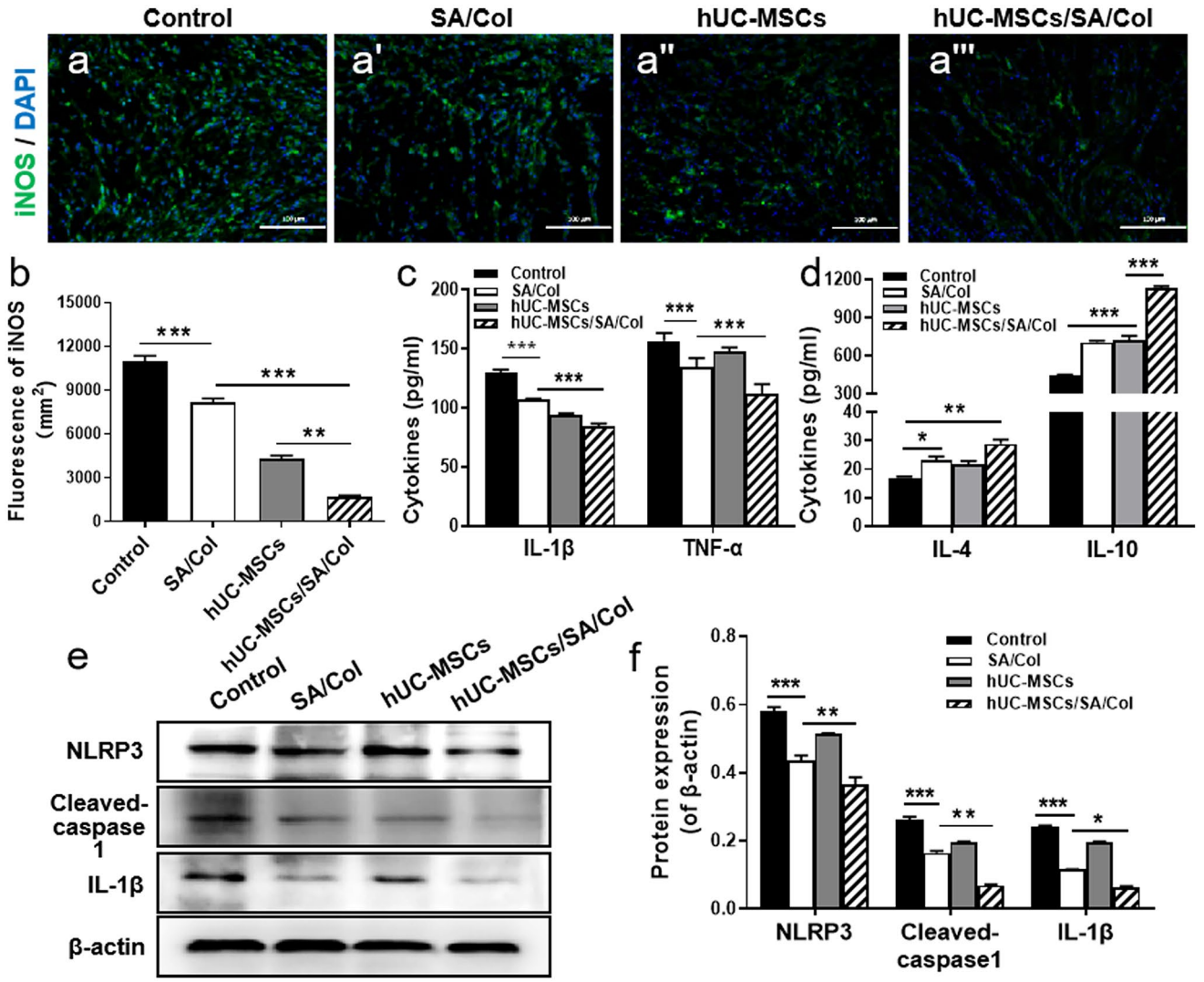

Fig. 8 SA/Col hydrogel loaded with hUC-MSCs inhibited inflammation and NLRP3 signaling. Representative images of iNOS immunohistochemistry staining (a-a'''), scale bar = 100 μm. Quantification analysis of iNOS fluorescence intensity (b). Quantitative analysis of the expression of TNF-α, IL-1β, IL-4, and IL-10 detected by ELISA in the serum (c, d). Representative images of relevant protein expressions in the injured skin tissue detected by Western blot (e). Quantitative analysis of the proteins expression associated with NLRP3 pathway (f). Data were presented as mean ± SD. $*p < 0.05$; $**p < 0.01$; $***p < 0.001$

inflammasome is a multi-protein complex formed by the combination of NLRP3 molecule, ASC and pro-caspase-1 (Bian et al. 2017). Under normal conditions, NLRP3 is dispersed in the cytoplasm. Once stimulated, NLRP3 binds to ASC, activates caspase-1 to induce self-cleavage, and then promotes the maturation and secretion of pro-inflammatory cytokines, such as IL-lβ (Elliott and Sutterwala 2016). Our results demonstrated that hUC-MSCs/SA/Col significantly inhibited the expressions of NLRP3, caspase-1, and IL-1β, which partially indicated that hUC-MSCs/SA/Col may promote wound healing by the inhibition of NLRP3 signaling. But, NLRP3 transgenic mice or rescue study should be carried out in the further study to examine the specific underlying molecular mechanism.

Conclusion

SA/Col hydrogel loaded with hUC-MSCs accelerates wound closure and tissue remodeling by promoting the survival of hUC-MSCs, enhancing growth factors secretion, and inhibiting inflammation response in the wound. The mechanisms may partially related to the inhibition of NLRP3 signaling pathway. In conclusion, SA/Col hydrogel contributes to better microenvironment for hUC-MSCs *in vivo* to improve its therapeutic effect in wound healing, which may provide a novel alternative approach to treat cutaneous wound.

Acknowledgments We thank all the members of Prof. Fangxia Guan's laboratory for the help and advice on this study.

Author contributions SS.M and FX.G conceived and designed the experiments. ZK.Z and SS.M wrote the manuscript. K.Z and MH.Y revised the final version of the paper. ZK.Z, Z.L and Y.L performed the experiments. YY.W, ZY.C, H.Y, and JJ.S prepared materials and analyzed the data. All authors reviewed the manuscript prior to submission.

Funding This study was supported by Key R&D and Promotion Projects in Henan Province (202102310211), Central Plains Thousand People Plan of Henan Province (204200510013), Training plan for young excellent teachers in Colleges and Universities of Henan (2020GGJS008), and Joint Fund for Fostering Talents of NCIR-MMT & HNKL-MMT (No. MMT2017-04).

Availability of data and materials The data that support the findings of this study are available from the corresponding author upon request.

Compliance with ethical standard

Ethical approval This study was approved by the Ethics Committees of the Zhengzhou University. All procedures involving human participants were conducted in accordance with the ethical standards of the Ethics Committees of the First Affiliated Hospital of Zhengzhou University. All the animal procedures were conducted in strict accordance with the National Institutes of Health guidelines for the Care and Use of Laboratory Animals.

Conflict of interest The authors declare that they have no conflict of interest.

Informed consent All applicable international, national, and/or institutional guidelines for the care and use of animals were followed. This study was approved by the Ethics Committees of the Zhengzhou University. All procedures involving human participants were conducted in accordance with the ethical standards of the Ethics Committees of the First Affiliated Hospital of Zhengzhou University. The human umbilical cords were obtained from healthy donors following full-term cesarean with prior informed consent.

References

Agabalyan NA, Sparks HD, Tarraf S, Rosin NL, Anker K, Yoon G, Burnett LN, Nickerson D, Di Martino ES, Gabriel VA, Biernaskie J (2019) Adult human dermal progenitor cell transplantation modulates the functional outcome of split-thickness skin xenografts. Stem Cell Reports 13:1068–1082

Bian F, Xiao Y, Zaheer M, Volpe EA, Pflugfelder SC, Li DQ, de Paiva CS (2017) Inhibition of NLRP3 inflammasome pathway by butyrate improves corneal wound healing in corneal alkali burn. Int J Mol Sci 18:

Chappell JC, Wiley DM, Bautch VL (2012) How blood vessel networks are made and measured. Cells Tissues Organs 195:94–107

Chen B, Kao HK, Dong Z, Jiang Z, Guo L (2017) Complementary effects of negative-pressure wound therapy and pulsed radiofrequency energy on cutaneous wound healing in diabetic mice. Plast Reconstr Surg 139:105–117

Chen S, Shi J, Zhang M, Chen Y, Wang X, Zhang L, Tian Z, Yan Y, Li Q, Zhong W, Xing M, Zhang L, Zhang L (2015) Mesenchymal stem cell-laden anti-inflammatory hydrogel enhances diabetic wound healing. Sci Rep 5:18104

Chin JS, Madden L, Chew SY, Becker DL (2019) Drug therapies and delivery mechanisms to treat perturbed skin wound healing. Adv Drug Deliv Rev 149–150:2–18

Dong Y, A S, Rodrigues M, Li X, Kwon SH, Kosaric N, Khong S, Gao Y, Wang W, Gurtner GC (2017) Injectable and tunable gelatin hydrogels enhance stem cell retention and improve cutaneous wound healing. Adv Func Mater 27:1606619

Dvorak HF (2015) Tumors: Wounds that do not heal-redux. Cancer Immunol Res 3:1–11

Elliott EI, Sutterwala FS (2016) Monocytes take their own path to IL-1beta. Immunity 44:713–715

Gao X, Gao L, Groth T, Liu T, He D, Wang M, Gong F, Chu J, Zhao M (2019) Fabrication and properties of an injectable sodium alginate/PRP composite hydrogel as a potential cell carrier for cartilage repair. J Biomed Mater Res A 107:2076–2087

Geng X, Hong Q, Chi K, Wang S, Cai G, Wu D (2019) Mesenchymal stem cells loaded with gelatin microcryogels attenuate renal fibrosis. Biomed Res Int 2019:6749326

Gilarska A, Lewandowska-Lancucka J, Guzdek-Zajac K, Karewicz A, Horak W, Lach R, Wojcik K, Nowakowska M (2019) Bioactive yet antimicrobial structurally stable collagen/chitosan/lysine functionalized hyaluronic acid - based injectable hydrogels for potential bone tissue engineering applications. Int J Biol Macromol

Goren I, Christen U, Pfeilschifter J, Frank S (2018) A heterogeneous Ly-6B2(+) leukocyte population consists of yet undescribed iNOS-expressing cell types in murine skin wounds. Nitric Oxide 74:23–31

Griffin DR, Weaver WM, Scumpia PO, Di Carlo D, Segura T (2015) Accelerated wound healing by injectable microporous gel scaffolds assembled from annealed building blocks. Nat Mater 14:737–744

Guan F, Huang T, Wang X, Xing Q, Gumpper K, Li P, Song J, Tan T, Yang GL, Zang X, Zhang J, Wang Y, Yang Y, Liu Y, Zhang Y, Yang B, Ma J, Ma S (2019) The TRIM protein Mitsugumin 53 enhances survival and therapeutic efficacy of stem cells in murine traumatic brain injury. Stem Cell Res Ther 10:352

Hersant B, Sid-Ahmed M, Braud L, Jourdan M, Baba-Amer Y, Meningaud JP, Rodriguez AM (2019) Platelet-rich plasma improves the wound healing potential of mesenchymal stem cells through paracrine and metabolism alterations. Stem Cells Int 2019:1234263

Huang P, Wang L, Li Q, Xu J, Xu J, Xiong Y, Chen G, Qian H, Jin C, Yu Y, Liu J, Qian L, Yang Y (2019) Combinatorial treatment of acute myocardial infarction using stem cells and their derived exosomes resulted in improved heart performance. Stem Cell Res Ther 10:300

Kamoun EA, Kenawy E-RS, Tamer TM, El-Meligy MA, Mohy Eldin MS (2015) Poly (vinyl alcohol)-alginate physically crosslinked hydrogel membranes for wound dressing applications: Characterization and bio-evaluation. Arabian Journal of Chemistry 8:38–47

Kasuya A, Tokura Y (2014) Attempts to accelerate wound healing. J Dermatol Sci 76:169–172

Li T, Xia M, Gao Y, Chen Y, Xu Y (2015) Human umbilical cord mesenchymal stem cells: An overview of their potential in cell-based therapy. Expert Opin Biol Ther 15:1293–1306

Liang Y, Walczak P, Bulte JW (2013) The survival of engrafted neural stem cells within hyaluronic acid hydrogels. Biomaterials 34:5521–5529

Liu B, Ding F, Hu D, Zhou Y, Long C, Shen L, Zhang Y, Zhang D, Wei G (2018) Human umbilical cord mesenchymal stem cell conditioned medium attenuates renal fibrosis by reducing inflammation and epithelial-to-mesenchymal transition via the TLR4/NF-kappaB signaling pathway in vivo and in vitro. Stem Cell Res Ther 9:7

Liu X, Long X, Liu W, Zhao Y, Hayashi T, Yamato M, Mizuno K, Fujisaki H, Hattori S, Tashiro SI, Ogura T, Atsuzawa Y, Ikejima T (2018) Type I collagen induces mesenchymal cell differentiation

into myofibroblasts through YAP-induced TGF-beta1 activation. Biochimie 150:110–130
Ma Z, Song W, He Y, Li H (2020) Multilayer injectable hydrogel system sequentially delivers bioactive substances for each wound healing stage. ACS Appl Mater Interfaces 12:29787–29806
Martin P (1997) Wound healing–aiming for perfect skin regeneration. Science 276:75–81
Marusina AI, Merleev AA, Luna JI, Olney L, Haigh NE, Yoon D, Guo C, Ovadia EM, Shimoda M, Luxardi G, Boddu S, Lal NN, Takada Y, Lam KS, Liu R, Isseroff RR, Le S, Nolta JA, Kloxin AM, Maverakis E (2020) Tunable hydrogels for mesenchymal stem cell delivery: Integrin-induced transcriptome alterations and hydrogel optimization for human wound healing. Stem Cells 38:231–245
Mushahary D, Spittler A, Kasper C, Weber V, Charwat V (2018) Isolation, cultivation, and characterization of human mesenchymal stem cells. Cytometry A 93:19–31
Nguyen NT, Nguyen LV, Tran NM, Nguyen DT, Nguyen TN, Tran HA, Dang NN, Vo TV, Nguyen TH (2019) The effect of oxidation degree and volume ratio of components on properties and applications of in situ cross-linking hydrogels based on chitosan and hyaluronic acid. Mater Sci Eng C Mater Biol Appl 103:109670
Rahimi M, Noruzi EB, Sheykhsaran E, Ebadi B, Kariminezhad Z, Molaparast M, Mehrabani MG, Mehramouz B, Yousefi M, Ahmadi R, Yousefi B, Ganbarov K, Kamounah FS, Shafiei-Irannejad V, Kafil HS (2020) Carbohydrate polymer-based silver nanocomposites: Recent progress in the antimicrobial wound dressings. Carbohydr Polym 231:115696
Rathinam VAK, Chan FK (2018) Inflammasome, inflammation, and tissue homeostasis. Trends Mol Med 24:304–318
Reynolds LE, Conti FJ, Lucas M, Grose R, Robinson S, Stone M, Saunders G, Dickson C, Hynes RO, Lacy-Hulbert A, Hodivala-Dilke K (2005) Accelerated re-epithelialization in beta3-integrin-deficient- mice is associated with enhanced TGF-beta1 signaling. Nat Med 11:167–174
Sakai S, Shichita T (2019) Inflammation and neural repair after ischemic brain injury. Neurochem Int 130:104316
Singer AJ, Clark RA (1999) Cutaneous wound healing. N Engl J Med 341:738–746
Spees JL, Lee RH, Gregory CA (2016) Mechanisms of mesenchymal stem/stromal cell function. Stem Cell Res Ther 7:125
Vallee A, Lecarpentier Y (2019) TGF-beta in fibrosis by acting as a conductor for contractile properties of myofibroblasts. Cell Biosci 9:98
Volz AC, Omengo B, Gehrke S, Kluger PJ (2019) Comparing the use of differentiated adipose-derived stem cells and mature adipocytes to model adipose tissue in vitro. Differentiation 110:19–28
Wang P, Huang S, Hu Z, Yang W, Lan Y, Zhu J, Hancharou A, Guo R, Tang B (2019) In situ formed anti-inflammatory hydrogel loading plasmid DNA encoding VEGF for burn wound healing. Acta Biomater 100:191–201
Wang X, Guan S, Zhang K, Li J (2020) Benlysta-loaded sodium alginate hydrogel and its selective functions in promoting skin cell growth and inhibiting inflammation. ACS Omega 5:10395–10400
Xu Q, A S, Gao Y, Guo L, Creagh-Flynn J, Zhou D, Greiser U, Dong Y, Wang F, Tai H, Liu W, Wang W, Wang W, (2018) A hybrid injectable hydrogel from hyperbranched PEG macromer as a stem cell delivery and retention platform for diabetic wound healing. Acta Biomater 75:63–74
Yao M, Zhang J, Gao F, Chen Y, Ma S, Zhang K, Liu H, Guan F (2019) New bmsc-laden gelatin hydrogel formed in situ by dual-enzymatic cross-linking accelerates dermal wound healing. ACS Omega 4:8334–8340
Zhang K, Shi Z, Zhou J, Xing Q, Ma S, Li Q, Zhang Y, Yao M, Wang X, Li Q, Li J, Guan F (2018) Potential application of an injectable hydrogel scaffold loaded with mesenchymal stem cells for treating traumatic brain injury. Journal of Materials Chemistry B 6:2982–2992
Zhao R, Liang H, Clarke E, Jackson C, Xue M (2016) Inflammation in Chronic Wounds. Int J Mol Sci 17:
Zhou J, Zhang K, Ma S, Liu T, Yao M, Li J, Wang X, Guan F (2019) Preparing an injectable hydrogel with sodium alginate and type I collagen to create better MSCs growth microenvironment. e-Polymers 19:87–91